



1 **Last ice sheet recession and landscape emergence above sea level in east-central Sweden, evaluated**
2 **using *in situ* cosmogenic ^{14}C from quartz**

3

4 Bradley W. Goodfellow^{1*}

5 Arjen P. Stroeven^{2,3}

6 Nathaniel A. Lifton^{4,5}

7 Jakob Heyman⁶

8 Alexander Lewerentz¹

9 Kristina Hippe⁷

10 Jens-Ove Näslund⁸

11 Marc W. Caffee^{4,5}

12

13 ¹Geological Survey of Sweden

14 ²Department of Physical Geography, Stockholm University

15 ³Bolin Centre for Climate Research, Stockholm University

16 ⁴Department of Earth, Atmospheric, and Planetary Sciences, Purdue University

17 ⁵Department of Physics and Astronomy, Purdue University

18 ⁶Department of Earth Sciences, University of Gothenburg

19 ⁷Umweltplanung Dr. Klimsa

20 ⁸Swedish Nuclear Fuel and Waste Management Company (SKB)

21

22 *Corresponding author: bradley.goodfellow@sgu.se

23

24 **Abstract**

25 *In situ* ^{14}C in quartz provides a recently developed tool to date exposure of bedrock surfaces up to
26 ~25 000 years. From outcrops located in east-central Sweden, we test the accuracy of *in situ* ^{14}C dating
27 against (i) a relative sea level (RSL) curve constructed from radiocarbon dating of organic material in
28 isolation basins, and (ii) the timing of local deglaciation constructed from a clay varve chronology
29 complemented with radiocarbon dating. Five samples of granitoid bedrock were taken along an
30 elevation transect extending southwestwards from the Baltic Sea coast near Forsmark. Because these
31 samples derive from bedrock outcrops positioned below the highest postglacial shoreline, they target
32 the timing of progressive landscape emergence above sea level. In contrast, *in situ* ^{14}C concentrations
33 in an additional five samples taken from granitoid outcrops above the highest postglacial shoreline,
34 located 100 km west of Forsmark, should reflect local deglaciation ages. The ten *in situ* ^{14}C



35 measurements provide robust age constraints that, within uncertainties, compare favorably with the
36 RSL curve and with the local deglaciation chronology. These data demonstrate the utility of *in situ* ^{14}C
37 to accurately date ice sheet deglaciation, and durations of postglacial exposure, in regions where
38 cosmogenic ^{10}Be and ^{26}Al routinely return complex exposure results.

39 **1. Introduction**

40 The pacing of retreat of ice sheets in North America and Eurasia since their maximum expansion
41 during the last glaciation remains an active research field (e.g., Hughes et al., 2016; Stroeven et al.,
42 2016; Patton et al., 2017; Dalton et al., 2020, 2023). Understanding the triggers and processes causing
43 the demise of these ephemeral ice sheets yields the best blueprint for understanding the future
44 behavior of the Greenland and Antarctic ice sheets in a warming climate. Coupling the behavior of
45 deglaciating ice sheets over the course of the Late Glacial and early Holocene to increasingly precise
46 climate reconstructions and climatic events, requires increased precision in ice sheet reconstructions
47 (e.g., Bradwell et al., 2021). Increased precision can be achieved through a coupling of
48 geomorphological mapping of ice sheet margins (such as moraines, grounding zone wedges, lateral
49 meltwater channels, and ice-dammed lake shorelines and spillways) with numerical field constraints
50 from a diverse array of dating techniques (e.g., Stroeven et al., 2016; Bradwell et al., 2021; Regnéll et
51 al., 2023).

52 Ice sheet reconstructions, especially in North America, have attained a high level of detail through
53 radiocarbon dating (Dyke et al., 2002; Dalton et al., 2020). With the advance of offshore imaging of
54 glacial geomorphology (Greenwood et al., 2017, 2021; Bradwell et al., 2021), radiocarbon dating has
55 received a renewed upswing in recent years (e.g., Dalton et al., 2020; Bradwell et al., 2021). However,
56 large tracts of landscape lack radiocarbon age constraints on ice sheet retreat simply due to a lack of
57 datable organic material. Fortunately, optically-stimulated luminescence ages on buried sand layers
58 (e.g., Alexanderson et al., 2022) and cosmogenic nuclide apparent exposure ages on exposed bedrock
59 and erratics have narrowed some of the gaps (e.g., Hughes et al., 2016; Stroeven et al., 2016; Dalton et
60 al., 2023). In studies using cosmogenic nuclides, an ‘apparent’ exposure age is derived from a simple
61 calculation from the nuclide concentration under consideration (Lal, 1991; Gosse and Phillips, 2001).
62 However, correctly interpreting the exposure age relies on modelling that considers geological factors
63 that can reduce the nuclide concentration relative to the time since initial subaerial exposure (such as
64 erosion and burial by glacial ice, water, snow, and/or soil; Gosse and Phillips, 2001; Schildgen et al.,
65 2005; Ivy-Ochs and Kober, 2008). Exposure dating is the only technique available in regions where ice
66 sheet erosion has left the surface bare or covered by a thin drape of till. Kleman et al. (2008) show that
67 for Fennoscandia, these conditions are widespread in coastal regions where ice accelerated towards its



68 streaming sectors and where wave wash during glacial rebound further thinned or removed pre-
69 existing sediment covers.

70 Coastal sectors in formerly glaciated regions provide sites important to the study of paleoglaciology.
71 They offer an abundance of bedrock exposures from which patterns and processes of subglacial
72 erosion can be studied through cosmogenic nuclide exposure dating (e.g., Hall et al., 2020). Also,
73 because of the interplay with postglacial sea level, coastal areas yield data on glacioisostatic rebound
74 that are critical to geodynamic modelling of Earth rheology and thicknesses of former ice sheets (e.g.,
75 Lambeck et al. (1998, 2010) and Patton et al. (2017), for Fennoscandian examples). Geodynamic
76 models require validation against measurements of vertical crustal motion (Steffen and Wu, 2011),
77 such as those provided by recent global positioning system (GPS) measurements (e.g., Lidberg et al.,
78 2010) and postglacial records of crustal rebound afforded by relative sea level (RSL) curves (e.g., Pässe
79 and Andersson, 2005). The construction of RSL curves, detailing the history of land surface emergence
80 from sea level, is traditionally done using either sediments accumulated in isolation basins at different
81 elevations above sea level or by dating uplifted gravel beach ridges. Typically, isolation basins, and their
82 sediments, show a progression from marine, to brackish, and finally to freshwater environments as
83 their bedrock sills are uplifted through tidal levels (Long et al., 2011). Histories of land uplift above sea
84 level are documented using micro- and macrofossil analyses of isolation basin sediments and
85 radiocarbon dating on macrofossils (Romundset et al., 2011). Uplifted beach ridges can be radiocarbon
86 dated from a variety of materials (Blake, 1993) but most confidently from driftwood, whalebone, and
87 shells (e.g., Dyke et al., 1992). Gravel beach ridges have also been investigated using OSL and ^{10}Be
88 exposure dating even though, other than the highest beach ridge, they may be prone to clast
89 reworking (Briner et al., 2006; Simkins et al., 2013; Bierman et al., 2018). A distinct advantage of
90 constructing RSL curves using cosmogenic nuclides is that land surface emergence above sea level may
91 be additionally dated from boulders (Briner et al., 2006) or bedrock (Bierman et al., 2018).

92 The potential for cosmogenic surface exposure dating of last ice sheet retreat in recently glaciated low-
93 relief cratonic landscapes would seemingly be high because of the frequent outcropping of glacially
94 sculptured quartz-bearing crystalline bedrock. However, the ice sheet may have been either non-
95 erosive or erosion was insufficiently deep to remove all the cosmogenic nuclide inventory from
96 previous exposure periods. Apparent ages are therefore often older than indicated by radiocarbon
97 dating (Heyman et al., 2011; Stroeven et al., 2016) because they include a component of nuclide
98 inheritance. Apparent ages younger than indicated by radiocarbon dating can also occur if sampled
99 rock surfaces have been shielded, for example by sediments, following deglaciation. Concentrations of
100 ^{10}Be and ^{26}Al , in either bedrock or erratic boulders, therefore often reflect complex exposure histories
101 rather than simple deglacial exposure durations (Heyman et al., 2011; Stroeven et al., 2016).



102 In this study we use ^{14}C produced *in situ* in quartz-bearing bedrock (*in situ* ^{14}C) because it potentially
103 circumvents an overt reliance on the need for deep erosion (> 3 m) to remove the inherited signal from
104 previous exposure periods (Gosse and Phillips, 2001). The reason for this is that, because of its short
105 half-life of 5700 ± 30 years, nuclide inheritance will have largely decayed away if ice sheet burial at
106 investigated sites during the last glacial phase (marine isotope stage 2; MIS2) exceeded 25-30 ka, that
107 is, ca. 5 half-lives (Briner et al., 2014).

108 Some studies assessing changes in glacier and ice sheet extents over Late Glacial to Holocene
109 timescales have used *in situ* ^{14}C (Miller et al., 2006; Fogwill et al., 2014; Hippe et al., 2014;
110 Schweinsberg et al., 2018; Pendleton et al., 2019; Young et al., 2021; Schimmelpfennig et al., 2022). In
111 such studies, *in situ* ^{14}C has been applied with other nuclides with longer half-lives, in particular ^{10}Be ,
112 to unravel complex histories of glacier advance and retreat (e.g., Goehring et al., 2011) and spatial
113 patterns in glacial erosion in mountainous terrain (e.g., Steinemann et al., 2021). However, extensive
114 regions formerly covered by ice sheets are characterized by low relief, low elevation terrain, and the
115 effectiveness of *in situ* ^{14}C in dating ice sheet retreat in these non-alpine settings and in quantifying
116 shoreline displacement from bedrock samples has not been previously assessed. The aim of this study
117 is therefore to validate the use of ^{14}C formed *in situ* in bedrock as a reliable chronometer by evaluating
118 its performance in duplicating (i) a previously-established Holocene RSL curve based on radiocarbon
119 dating (Hedenström and Risberg, 2003; SKB, 2020) and (ii) the timing of deglaciation above the highest
120 (post-glacial) shoreline in nearby east-central Sweden according to reconstructions of deglaciation of
121 the last ice sheet (Hughes et al., 2016; Stroeven et al., 2016).

122

123 2. Study Area

124 Our study is focused on a region that includes low elevation, low relief, Forsmark-Uppland and
125 adjoining higher elevation and relief Dalarna-Gävleborg in east-central Sweden (Fig. 1). This region was
126 selected because Forsmark is the location of a planned geological repository for spent nuclear fuel
127 (e.g., SKB 2022) and therefore also has abundant geologic data relevant to our study. This includes in-
128 depth analyses of bedrock and environmental properties, including influences of glacial and postglacial
129 processes (e.g., Lönnqvist and Hökmark, 2013; Hall et al., 2019; Moon et al., 2020; SKB, 2020).

130 From spatio-temporal ice sheet reconstructions by Kleman et al. (2008), the study area was glaciated
131 16-20 times for a total duration of c. 330 ky over the past 1 Ma. The last deglaciation of the study area
132 is well-constrained by two recent reconstructions that differ in their approach (Hughes et al., 2016;
133 Stroeven et al., 2016). The Hughes et al. (2016) reconstruction is explicitly based on chronological
134 constraints, but the Stroeven et al. (2016) reconstruction combines geomorphological constraints for
135 ice sheet margin outlines with chronological constraints. Whereas Hughes et al. (2016) reconstruct ice



136 sheet retreat every 1 ka, and for every ice margin plot its position as “most credible”, “min”, and
137 “max”, Stroeven et al. (2016) present ice margin positions for every 100 years inside the Younger Dryas
138 standstill position (Stroeven et al., 2015). These marginal positions are temporally and spatially defined
139 by the “Swedish Time Scale” clay varve record along the Swedish east coast (De Geer, 1935, 1940;
140 Strömberg, 1989, 1994; Brunnberg, 1995; Wohlfarth et al., 1995). From Stroeven et al. (2016), the last
141 deglaciation of the study area occurred 10.8 ± 0.3 ka BP, which overlaps the timing of deglaciation of
142 the study area from Hughes et al. (2016), within uncertainty (Fig. 1). The highest postglacial shoreline
143 in east-central Sweden is located at a present elevation of ~ 200 m a.s.l. in Dalarna-Gävleborg, ~ 100 km
144 west of Forsmark (SGU, 2015). The exposure duration of bedrock above the highest postglacial
145 shoreline therefore represents the time since local deglaciation. Hence, *in situ* ^{14}C ages from bedrock
146 above the highest postglacial shoreline should conform to the reconstructed deglaciation age of $10.8 \pm$
147 0.3 ka from Stroeven et al. (2016).

148 Below the highest postglacial shoreline, in the Forsmark-Uppland region, the last deglaciation
149 occurred in a marine environment and the landscape has progressively emerged above sea level
150 through postglacial isostatic uplift. A RSL curve constructed from radiocarbon dating of basal organic
151 sediments trapped in isolation basins along elevation transects describes the progressive emergence
152 of the Forsmark-Uppland landscape above sea level (Robertsson and Persson, 1989; Risberg, 1999;
153 Bergström, 2001; Hedenström and Risberg, 2003; Berglund, 2005; SKB, 2020). Ages calculated from *in*
154 *situ* ^{14}C from bedrock outcrops along an elevation transect would then mirror the Forsmark RSL curve
155 for their corresponding elevations (but be slightly older because of nuclide production through
156 shallow water before emergence).

157 A potential complication to the accurate exposure age dating of bedrock surfaces using *in situ* ^{14}C in
158 east-central Sweden is that the most recent period of ice sheet burial may not have been sufficiently
159 long to decay the *in situ* ^{14}C inventory inherited from preceding exposure. Here, the extent of the
160 Fennoscandian Ice Sheet during interstadial MIS3 and the timing of ice advance across the Forsmark
161 region during late MIS3 are crucially important. Kleman et al. (2020) have identified ice-free conditions
162 around Idre (330 km NW, up-ice, of our study area; Fig. 1) between 55 ka and 35 ka, which implies
163 inundation of our study area by ice after 35 ka. Combined with a well-constrained final deglaciation
164 age of 10.8 ± 0.3 ka (Stroeven et al. 2016), it appears that our study area has most recently (during
165 MIS2) been inundated by glacial ice for at most 24 ka. This inference is in line with results from ice
166 sheet modelling indicating a 22 kyr duration of ice-cover at Forsmark during MIS2 (SKB, 2020).
167 Consequently, it is possible that *in situ* ^{14}C concentrations may reflect subaerial exposure of bedrock in
168 our study area during MIS3 in addition to Holocene exposure, resulting in an offset towards older ages
169 relative to the RSL curve for Forsmark (Hedenström and Risberg, 2003; SKB, 2020) and the deglaciation
170 chronologies of Hughes et al. (2016) and Stroeven et al. (2016).



171

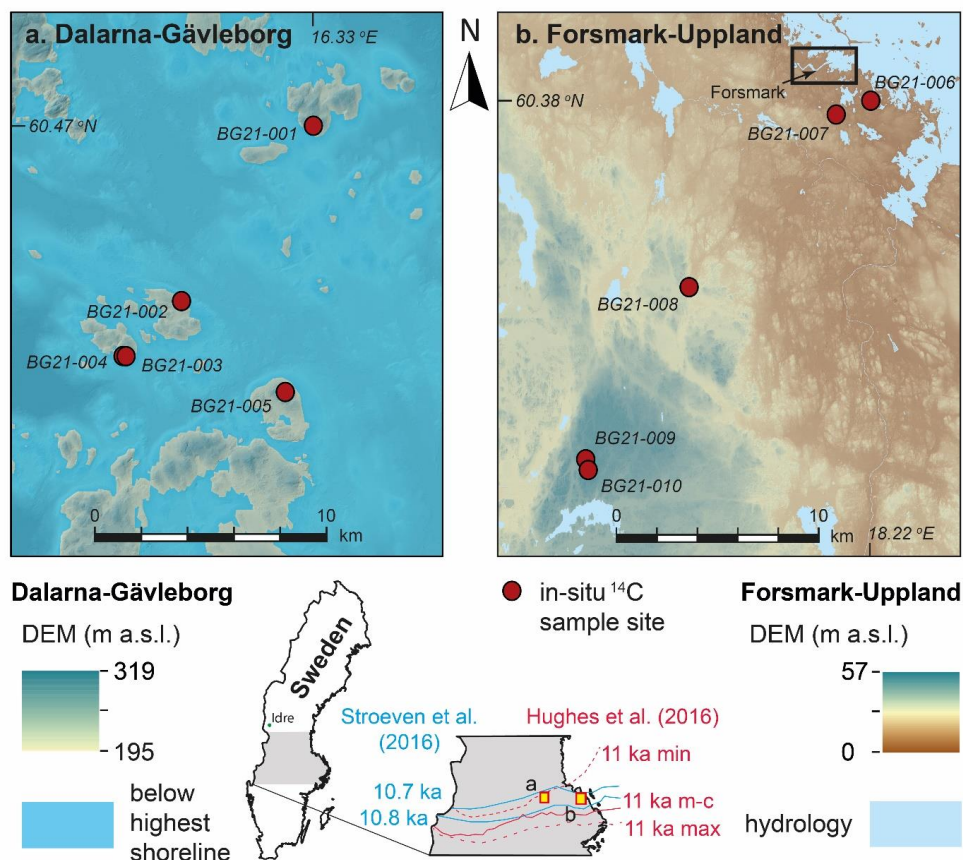
172 3. Methods

173 3.1. Sampling of bedrock outcrops for *in situ* ¹⁴C measurement

174 We used the following sampling strategy to evaluate the accuracy of bedrock exposure ages derived
175 from *in situ* ¹⁴C against the Forsmark RSL curve and the deglaciation of the last ice sheet in east-central
176 Sweden. A rigorous scheme was applied to ensure that we avoided sampling quartz altered through
177 hydrothermal processes that is likely to occur in major pegmatite intrusions, outcrops located in major
178 deformation zones, and outcrop-scale veins, fractures, and adjacent rock volumes. Consequently,
179 sampling was done on outcrops of metagranitoid from the early-Svecokarelian GDG-GSDG suite that
180 dominates the Bergslagen lithotectonic unit (Stephens and Jansson, 2020). A petrological examination
181 using transmitted light polarization microscopy was applied to thin sections to ascertain that the quartz
182 was unlikely to contain multi-fluid phase, vapour phase, or solid-phase inclusions. All samples were
183 collected using an angle grinder, which permits sampling of hard crystalline bedrock isolated from
184 outcrop edges, fractures, and quartz veins, and consistently limits sample thicknesses to 3 cm.

185 We collected a total of ten samples for *in situ* ¹⁴C analyses. Five of these were collected along a SW-NE
186 transect near Forsmark (Fig. 1b). These outcrops were chosen because they span an elevation gradient
187 of 9.4–56.0 m a.s.l. and exposure ages derived from *in situ* ¹⁴C can therefore be evaluated against the
188 Forsmark RSL curve. We collected a further five samples from locations above the highest shoreline (Fig.
189 1a) to determine the age of local deglaciation for comparison with published deglaciation chronologies
190 (Hughes et al., 2016; Stroeven et al., 2016). Sample locations were logged on a 2 m-resolution LiDAR
191 digital elevation model (DEM) displayed in ArcGIS 10 on a tablet computer. A GPS add-in tool in ArcGIS
192 10 was used to record positional data, within a horizontal precision of 2 m. The elevation of each sample
193 location was extracted from the DEM and has a precision of tens of centimetres. The influence of these
194 minor positional uncertainties on our ¹⁴C calculations is trivial and none of the sample sites is influenced
195 by topographic shielding that could reduce the accumulation of ¹⁴C in bedrock.

196 Each sampled bedrock outcrop formed a local topographic high, which minimizes the risk of burial by
197 soil and snow (Supplement 1). Moss mats were present on all sampled outcrops. Although we avoided
198 sampling bedrock that was moss-covered, we cannot be certain that moss mats did not formerly cover
199 the sample sites. Given a compressed thickness of 0.5 cm and an estimated density of 0.7 g/cm³, this
200 may have contributed to a shielding of the sampled rock surfaces of 0.35 g/cm², which is negligible and
201 is therefore excluded from our age inferences.



202

203 **Figure 1.** Sample locations for *in situ* ^{14}C dating in (a) Dalarna-Gävleborg and (b) Forsmark-Uppland. The
204 five Dalarna-Gävleborg sample sites are located above the highest postglacial shoreline (shown),
205 whereas the five sample sites from Forsmark-Uppland are located below the highest shoreline (not
206 shown because the entire area was submerged). See inset maps for locations of panels a and b and for
207 the 10.7 ka BP and 10.8 ka BP retreat isochrones (blue) from Stroeven et al. (2016) and 11 ka BP (most-
208 credible, minimum, and maximum) retreat isochrones (red) from Hughes et al. (2016). The rectangle in
209 panel b approximately indicates the site selected for the planned geological repository for spent nuclear
210 fuel at Forsmark. DEM with 2 m resolution, from LiDAR data, Lantmäteriet.

211 3.2. Laboratory preparation for accelerator mass spectrometry (AMS)

212 Samples were physically and chemically processed at the Purdue Rare Isotope Measurement Laboratory
213 (PRIME Lab) at Purdue University, U.S.A. Concentrations of *in situ* ^{14}C were determined from purified
214 quartz separates through automated procedures (Lifton et al., 2023). Approximately 5 g of quartz from
215 each sample was added to a degassed LiBO_2 flux in a re-usable 90% Pt/10% Rh sample boat and heated

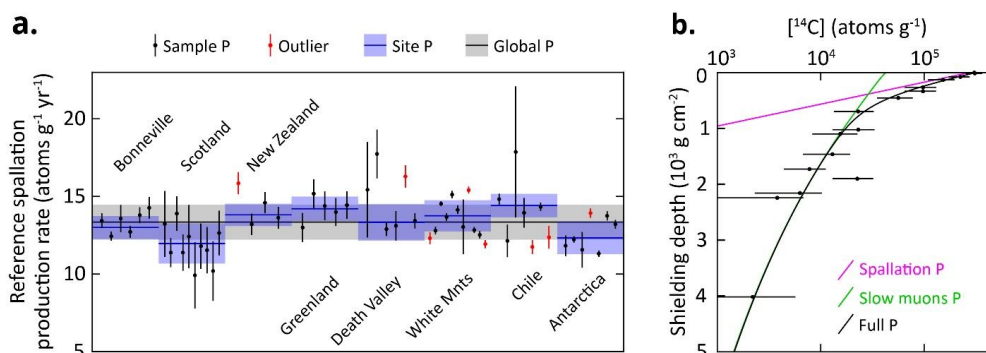


216 to 500 °C for one hour in ca. 6.7 kPa of Research Purity O₂ to remove atmospheric contaminants, which
217 were discarded. The sample was then heated to 1100 °C for three hours to dissolve the quartz and
218 release the *in situ* ¹⁴C, again in an atmosphere of ca. 6.7 kPa of Research Purity O₂ to oxidize any evolved
219 carbon species to CO₂. The CO₂ from the 1100 °C step was then purified, measured quantitatively, and
220 converted to graphite for ¹⁴C AMS measurement at PRIME Lab (Lifton et al., 2023). To test for data
221 reproducibility, sample BG21-002 was randomly selected to undergo laboratory preparation and AMS a
222 second time. Measured concentrations of *in situ* ¹⁴C are calculated from the measured isotope ratios via
223 AMS following Hippe and Lifton (2014).

224 3.3. Exposure age calculations

225 The expage calculator version 202312 (<http://expage.github.io/calculator>) is used to calculate apparent
226 exposure ages. It is based on the original CRONUS calculator v. 2 (Balco et al., 2008), the LSDn production
227 rate scaling (Lifton et al., 2014), and the CRONUScalc calculator (Marrero et al., 2016), using the
228 geomagnetic framework of Lifton (2016) with the SHA.DIF.14k model for the last 14 kyr. Exposure ages
229 are calculated using resulting time-varying ¹⁴C production rates accounting for decay and interpolated
230 to match the measured ¹⁴C concentration. The production rate from muons is calibrated against the
231 Leymon High core ¹⁴C data of Lupker et al. (2015) and the production rate from spallation is calibrated
232 against updated global ¹⁴C production rate calibration data (Schimmelpfennig et al., 2012; Young et al.,
233 2014; Lifton et al., 2015; Borchers et al., 2016; Phillips et al., 2016; Koester and Lifton, 2023). This
234 calibration is done iteratively for spallation and muons to reach convergence, using the expage
235 production rate calibration methods (Fig. 2).

236 Exposure age calculations along the Forsmark-Uppland transect account for ¹⁴C production during
237 emergence through shallow water. However, burial of sampled surfaces by snow is excluded from the
238 age calculations for all sample sites because we neither know how snow burial depths and durations
239 vary between sites nor vary through time. The effect of snow burial would be to slightly decrease
240 cosmogenic nuclide production in the underlying rock surface (Schildgen et al., 2005) and we have
241 minimized this effect through our sampling strategy.



242 **Figure 2.** Production rate calibration of ^{14}C in quartz. **(a)** Reference spallation ^{14}C production rate
243 calibration based on data from Schimmelpfennig et al. (2012), Young et al. (2014), Lifton et al. (2015),
244 Borchers et al. (2016), and Phillips et al. (2016), corrected per Hippe and Lifton (2014) and compiled in
245 Koester and Lifton (2023). An uncertainty-weighted production rate is calculated for each of the eight
246 sites. Outliers, which are not included in the uncertainty-weighted production rates, are determined
247 based on the requirement that there should be at least three samples yielding a reduced chi-square
248 statistic (χ^2_R) with a p-value of at least 0.05 for the assumption that the individual production rates from
249 a site are derived from one normal distribution. For χ^2_R , but not the uncertainty-weighting, we use the
250 largest of the sample-specific production rate uncertainty based on the ^{14}C concentration uncertainties
251 and 5% of the sample production rate. This procedure does not punish samples with low measurement
252 uncertainties, which otherwise risk exclusion as outliers. We adopt a global reference spallation ^{14}C
253 production rate of 13.35 ± 1.13 atoms $\text{g}^{-1} \text{yr}^{-1}$, calculated as the arithmetic mean of the eight site
254 production rates with the uncertainty being based on an uncertainty-weighted deviation of all included
255 single sample production rates, excluding outliers. **(b)** Calibration of ^{14}C production rate from muons
256 based on the data of Lupker et al. (2015). The calibration is based on the method used in the CRONUScal
257 calculator (Marrero et al., 2016; Phillips et al., 2016). The figure shows the best fit ^{14}C concentration
258 profiles produced from spallation, slow muons, and full production. The best fit yields near zero
259 production from fast muons (cf. Lupker et al., 2015). The production rate calibration has been carried
260 out using the expage-202306 calculator in an iterative way to make the global reference spallation ^{14}C
261 production rate converge with the production rate from muons.

262

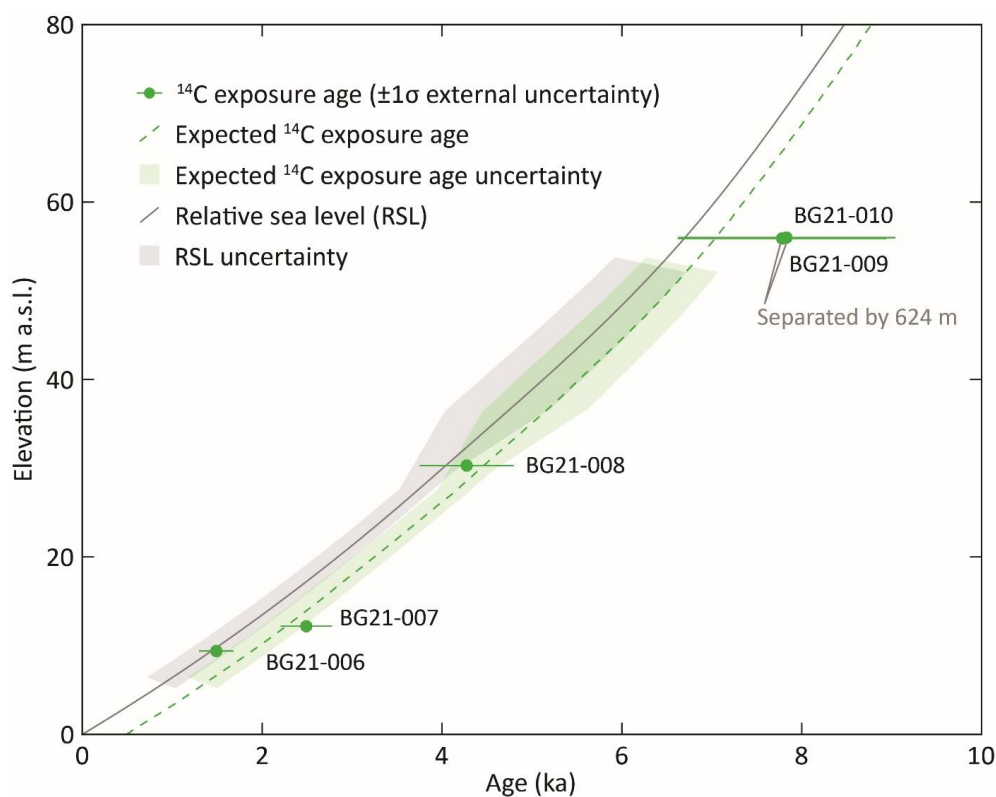
263 4. Results

264 Inferred ages for the five *in situ* ^{14}C samples from the Forsmark-Uppland transect (i.e., below the highest
265 postglacial shoreline) are shown relative to the Holocene RSL curve for Forsmark and the expected *in*
266 *situ* ^{14}C exposure age curve considering subaqueous cosmogenic nuclide production (Figure 3; Tables 1
267 and 2). Exposure age uncertainties are large with internal uncertainties (measurement uncertainties;



268 Balco et al., 2008) of 5-9% and external uncertainties of 12-20% (also including production rate
269 uncertainties, which are high relative to ^{10}Be (Borchers et al., 2016; Phillips et al., 2016). Apparent
270 exposure ages increase consistently with elevation and match expected ages within uncertainty. The two
271 highest samples have near-identical apparent exposure ages and elevations. However, these samples
272 provide independent ages because they are horizontally separated by 624 m (Figure 1b). There is good
273 agreement between ages inferred from these *in situ* ^{14}C data and the RSL curve constructed from organic
274 radiocarbon dating of isolation events (Hedenström and Risberg, 2003; SKB, 2020).

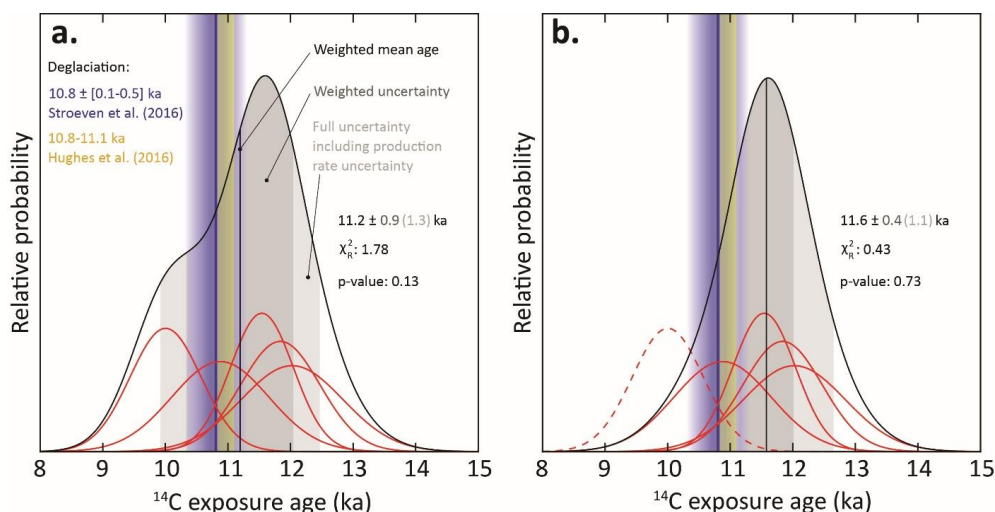
275



276 **Figure 3.** Apparent ^{14}C exposure ages for five Forsmark samples from below the highest shoreline (Fig.
277 1b; Table 2) with 1σ external uncertainties. The expected exposure ages are calculated assuming the RSL
278 curve is correct, the ^{14}C spallation production rate is correct, partial exposure as the sample approaches
279 the water surface, and full post-glacial exposure for the duration above sea level. Hence, the expected
280 exposure age curve is a few hundred years older than the RSL curve. The RSL curve is from SKB (2020)
281 and uncertainties for the 1–6 ka interval are calculated from the original radiocarbon data in Hedenström
282 and Risberg (2003). The RSL uncertainty envelope is also transposed onto the expected exposure age
283 curve.



284 Apparent exposure ages for the five *in situ* ^{14}C samples located above the highest shoreline in Dalarna
285 and Gävleborg (Fig. 1a) are shown in Figure 4 and Table 2. The weighted mean age from all five samples
286 is 11.2 ± 1.3 ka. These data display a X_R^2 of 1.78 and a p-value of 0.13 based on 1σ internal uncertainties
287 (Fig. 4a), which does not support a rejection of the hypothesis that the apparent exposure ages represent
288 the same population. In addition to the samples being from the same population, the exposure ages are
289 consistent, within uncertainty, with the expected deglaciation age of 10.8 ± 0.3 ka (Stroeven et al. 2016).
290 Replicate measurements on sample BG21-002 closely agree and an age based on a weighted mean ^{14}C
291 concentration is shown in Figure 4. Sample BG21-001 provides the youngest apparent age but, because
292 this sample was from a low-profile outcrop (Supplement 1), this age may reflect partial shielding of the
293 sampled bedrock surface by a past shallow soil cover or perhaps a deeper snow cover than the other
294 sites. We therefore consider this sample as least likely to provide a reliable age. Removing this sample
295 from consideration indicates that the remaining four sample sites are more clustered, with an older
296 weighted mean age of 11.6 ± 1.1 ka, which displays a X_R^2 of 0.43 and a p-value of 0.73 based on 1σ
297 internal uncertainties (Fig. 4b).
298



299 **Figure 4.** Probability density plots of the exposure ages from samples above the highest shoreline (Fig.
300 1a; Table 2). The individual samples (red curves) display 1σ internal uncertainty (measurement
301 uncertainty). For the repeat sample BG21-002, the exposure age is calculated with a weighted mean ^{14}C
302 concentration using a 2% uncertainty. **(a)** The probability density and data for all five samples. For the
303 full set of samples, the cosmogenic nuclide ages yield a reduced chi-square (X_R^2) of 1.78 and a p-value
304 of 0.13 based on internal uncertainties, which indicates that they are from the same population. **(b)** The
305 probability density and data with sample BG21-001 excluded as an outlier. These cosmogenic nuclide
306 ages yield a X_R^2 of 0.43 and a p-value of 0.73 based on internal uncertainties, which again indicate that



307 they are from the same population. All ages are referenced to the sampling year 2021. The weighted
308 ages of 11.2 ± 1.3 ka and 11.6 ± 1.1 ka both overlap with the deglaciation age from Stroeven et al. (2016).



Table 1. Extraction and measurement of *in situ* ¹⁴C at PRIME Lab.

Sample ID	PCEGS # ^a	PLID ^b	Mass Quartz (g)	C yield (μ g)	Diluted mass C (μ g)	AMS Split Mass C (μ g)	$\delta^{13}\text{C}$ (‰ _{vPDB})	¹⁴ C/ ¹³ C (10^{-11})	¹⁴ C/ ¹² C _{total} (10^{-13})	¹⁴ C (10^6 at)	[¹⁴ C] (10^6 at g^{-1}) ^c
BG21-001	146	202101960	5.02378	5.0 ± 0.1	393.8 ± 4.8	382.3 ± 4.6	-4.9 ± 0.2	0.3399 ± 0.0075	0.3412 ± 0.0079	0.6177 ± 0.0179	1.2296 ± 0.0357
BG21-002	147	202101961	5.02383	7.8 ± 0.1	303.3 ± 3.7	294.4 ± 3.6	-4.8 ± 0.2	0.4555 ± 0.0096	0.4623 ± 0.0102	0.6470 ± 0.0181	1.2879 ± 0.0360
BG21-003	148	202101962	5.01070	17.6 ± 0.3	303.4 ± 3.7	294.5 ± 3.6	-4.9 ± 0.2	0.4633 ± 0.0108	0.4709 ± 0.0113	0.6604 ± 0.0197	1.3180 ± 0.0393
BG21-002R	150	202201473	5.04116	7.7 ± 0.1	305.3 ± 3.7	296.4 ± 3.6	-4.5 ± 0.2	0.4568 ± 0.0135	0.4624 ± 0.0142	0.6519 ± 0.0237	1.2931 ± 0.0470
BG21-004	152	202101963	5.05927	11.9 ± 0.2	305.7 ± 3.7	296.8 ± 3.6	-4.6 ± 0.2	0.4618 ± 0.0079	0.4691 ± 0.0083	0.6630 ± 0.0159	1.3105 ± 0.0314
BG21-005	153	202101964	5.07578	4.6 ± 0.1	304.5 ± 3.7	295.6 ± 3.6	-4.5 ± 0.2	0.4600 ± 0.0127	0.4667 ± 0.0134	0.6566 ± 0.0225	1.2935 ± 0.0444
BG21-006	155	202101965	5.06572	5.5 ± 0.1	306.8 ± 3.7	297.8 ± 3.6	-4.5 ± 0.2	0.4277 ± 0.0056	0.1172 ± 0.0059	0.1243 ± 0.0101	0.2453 ± 0.0199
BG21-007	157	202101966	5.03589	6.9 ± 0.1	309.2 ± 3.8	300.1 ± 3.7	-4.5 ± 0.2	0.1684 ± 0.0051	0.1601 ± 0.0054	0.1922 ± 0.0096	0.3817 ± 0.0191
BG21-008	158	202101967	5.07653	4.0 ± 0.1	308.9 ± 3.8	299.9 ± 3.6	-4.5 ± 0.2	0.2357 ± 0.0063	0.2308 ± 0.0067	0.3015 ± 0.0119	0.5938 ± 0.0234
BG21-009	160	202101968	5.01906	55.3 ± 0.7	305.6 ± 3.7	296.6 ± 3.6	-3.8 ± 0.2	0.3339 ± 0.0095	0.3368 ± 0.0101	0.4601 ± 0.0170	0.9168 ± 0.0339
BG21-010	161	202101969	4.99961	42.2 ± 0.6	306.0 ± 3.7	297.0 ± 3.6	-4.0 ± 0.2	0.3320 ± 0.0068	0.3340 ± 0.0072	0.4565 ± 0.0132	0.9130 ± 0.0264

^a PCEGS # = sample number in the Purdue Carbon Extraction and Graphitization System

^b PLID = PRIME Lab ID

^c Measurement uncertainty of ± 0.2 ‰_{vPDB} (where VPDB is Vienna Pee Dee Belemnite)

^d Corrected for procedural blank of $(5.5952 \pm 0.3713) \times 10^{-4}$ atoms

309
310
311
312
313
314
315
316
317
318
319
320
321
322
323
324
325
326
327
328
329
330
331
332
333
334
335
336
337
338
339
340
341



Table 2. *In situ* ¹⁴C from quartz, Dalarna-Gävleborg and Forsmark-Upland.

Sample ID	Lat (°)	Long (°)	Elevation (m a.s.l.)	Thickness (cm)	Density (g cm ⁻³)	Shielding factor	Erosion (cm yr ⁻¹)	¹⁴ C ± 1σ (10 ² at g ⁻¹)	¹⁴ C Age ± Unc. Ext. (± Unc. Int.) ^a (ka)
BG21-001	60.47432	16.33134	236.5	3	2.7	1	0	1230 ± 36	10.0 ± 1.7 (± 0.6)
BG21-002	60.40615	16.22197	212.6	3	2.7	1	0	1288 ± 36	11.5 ± 2.2 (± 0.7)
BG21-002R	60.40615	16.22197	212.6	3	2.7	1	0	1293 ± 47	11.6 ± 2.3 (± 0.9)
BG21-003	60.38459	16.17649	216.3	3	2.7	1	0	1318 ± 39	12.0 ± 2.4 (± 0.8)
BG21-004	60.38451	16.17440	217.8	3	2.7	1	0	1311 ± 31	11.8 ± 2.3 (± 0.6)
BG21-005	60.36888	16.30526	248.1	3	2.7	1	0	1294 ± 44	10.9 ± 2.1 (± 0.8)
BG21-006	60.38490	18.22308	9.4	3	2.7	1	0	245 ± 20	1.5 ± 0.2 (± 0.1)
BG21-007	60.37892	18.19129	12.2	3	2.7	1	0	382 ± 19	2.5 ± 0.3 (± 0.1)
BG21-008	60.30504	18.04993	30.3	3	2.7	1	0	594 ± 23	4.3 ± 0.5 (± 0.2)
BG21-009	60.22988	17.94989	56.0	3	2.7	1	0	917 ± 34	7.8 ± 1.2 (± 0.5)
BG21-010	60.22431	17.95051	55.9	3	2.7	1	0	913 ± 26	7.8 ± 1.2 (± 0.4)

^a Unc. Ext. is external uncertainty and Unc. Int. is internal uncertainty. Both are 1σ.

342
343
344
345
346
347
348
349
350
351
352
353
354
355
356
357
358
359
360
361
362
363
364
365
366
367



368 **5. Discussion**

369 The *in situ* ^{14}C bedrock exposure ages from the Forsmark-Uppland transect (i.e., below the highest
370 postglacial shoreline) consistently increase with elevation and overlap the expected exposure age
371 curve, within uncertainty (Fig. 3). Because the apparent exposure ages accurately reflect the timing of
372 landscape emergence, *in situ* ^{14}C is indicated as having high potential as a chronometer over Late
373 Glacial-Holocene timescales in low relief, low elevation settings. This study adds to precious few
374 demonstrations of the ability of cosmogenic nuclide isotopes to define postglacial landscape
375 emergence above sea level (Briner et al., 2006; Bierman et al., 2018). Briner et al. (2006) present good
376 (visual) congruence with a record of shoreline emergence built from radiocarbon-dated driftwood and
377 fauna by Dyke et al. (1992) using ^{10}Be measurements on boulders in beaches derived from wave-
378 washed till. Their study also mentions that building a relative sea level curve from pebbles, cobbles and
379 plucked bedrock suffered from inheritance problems, an experience shared by Matmon et al. (2003)
380 while attempting the dating of chert on beach ridges in southern Israel and heeded by Bierman et al.
381 (2018). Bierman et al. (2018) successfully dated landscape emergence on Greenland using ^{10}Be across
382 a range of settings, including bedrock below the highest shoreline, cobbles from beach ridges at the
383 highest shoreline, and boulders and bedrock above the highest shoreline. They note that success hinges
384 on the requirement of warm-based ice and deep glacial erosion in exposing bedrock devoid of an
385 inherited cosmogenic nuclide inventory. In many regions, however, including east-central Sweden and
386 more widely in Fennoscandia, these requirements are not met either because of cold-based conditions
387 (Patton et al., 2016; Stroeven et al., 2016) or weakly erosive warm-based ice such as at Forsmark (Hall
388 et al., 2019; SKB, 2020), during all or much of glacial time. Cosmogenic nuclide inheritance is therefore
389 a part of the landscape fabric. Bierman et al. (2018) advocate the use of *in situ* ^{14}C as a methodology
390 to circumvent inheritance problems. Our study is the first to follow-up on that suggestion, and shows,
391 convincingly, that using *in situ* ^{14}C can extend the study of landscape rebound to regions where ice
392 sheet erosion was insufficiently deep to allow for the application of long-lived nuclides.

393 Five bedrock samples from above the highest postglacial shoreline are well-clustered and the weighted
394 mean age (and full uncertainty) of 11.2 ± 1.3 ka overlaps with the predicted deglaciation age of $10.8 \pm$
395 0.3 ka (Fig. 4a; Hughes et al., 2016; Stroeven et al., 2016). Removing the youngest age from
396 consideration results in more strongly clustered ages (Fig. 4b) and an older mean weighted age of 11.6
397 ± 1.1 ka, which still overlaps the predicted deglaciation age, within uncertainty. We therefore do not
398 further discriminate between these results. Because derived exposure ages overlap with the predicted
399 deglaciation age, we further infer that the *in situ* ^{14}C samples, including those located below the highest
400 postglacial shoreline, within uncertainty, lack inheritance from previous exposure. This implies that the
401 last ice sheet advanced over the study area soon after 35 ka, in accordance with previous inferences



402 for Forsmark (SKB, 2020). An alternative interpretation is that the last ice sheet advanced more recently
403 but that glacial erosion during MIS2 was sufficiently deep to remove any nuclide inheritance.

404 Our *in situ* ^{14}C data from above the highest (postglacial) shoreline demonstrate good potential for this
405 nuclide to help constrain the deglaciation chronology of former ice sheets. This is especially true for
406 regions with thin drift, abundant bedrock exposures, and lacking moraines outlining successive retreat
407 stages. In Fennoscandia, thin drift conditions occur commonly (cf. Kleman et al., 2008) and ice sheet
408 retreat appears to have proceeded uninterrupted inside the Younger Dryas moraine belt (apart from
409 the Central Finland Ice-Marginal Formation; e.g., Rainio et al., 1986; Stroeven et al., 2016). Whereas
410 the post-Younger Dryas deglaciation of east-central Sweden is well constrained by clay-varve
411 chronology (Strömberg, 1989) below the highest postglacial shoreline, there are vast areas above the
412 highest shoreline that remain poorly constrained by data (Stroeven et al. 2016). In addition to a lack of
413 datable deglacial landforms, this is attributable to glacial erosion of bedrock having frequently been
414 insufficient to remove inventories of long half-life ^{10}Be and ^{26}Al (Patton et al., 2022), thereby leaving
415 nuclides inherited from exposure prior to the last glaciation (Heyman et al., 2011; Stroeven et al., 2016).
416 Because of the short ^{14}C half-life and an improved sampling methodology, *in situ* ^{14}C may now be a
417 prime candidate nuclide to be included in last deglaciation studies on glaciated cratons, such as the
418 dating of boulders deposited along glacial flowlines; a technique practiced successfully using ^{10}Be
419 (Margold et al., 2019; Norris et al., 2022).

420

421 6. Conclusion

422 Ten *in situ* ^{14}C measurements on bedrock are consistent with a RSL curve for Forsmark derived from
423 organic radiocarbon dating of basal sediments in isolation basins and the Fennoscandian Ice Sheet
424 deglaciation chronologies from Stroeven et al. (2016) and Hughes et al. (2016). This study introduces
425 the use of *in situ* ^{14}C in Fennoscandian Ice Sheet paleoglaciology and outlines a promise of its use as a
426 basis for supporting future shoreline displacement studies and for tracking the deglaciation in areas
427 that lack datable organic material and where ^{10}Be and ^{26}Al routinely return complex exposure results.

428

429 **Data availability.** Data are available in Supplements 1-3. LiDAR data used in the study can
430 be downloaded from <https://www.lantmateriet.se>

431 **Author contributions.** BWG and APS initiated the study, with support from KH and JON, and drafted
432 the manuscript. BWG, APS, and AL did the sampling. AL did petrological analyses of the sampled
433 bedrock. NAL completed sample preparation for AMS and provided the results. JH carried out
434 cosmogenic nuclide production rate and exposure age calculations. MWC oversaw the AMS. All
435 authors revised the manuscript.



436 **Competing interests.** The contact author has declared that none of the authors has any competing
437 interests.

438 **Disclaimer.** Publisher's note: Copernicus Publications remains neutral with regard to jurisdictional
439 claims in published maps and institutional affiliations.

440 **Acknowledgements.** We thank Johan Liakka (SKB) for his support in completing this study.

441 **Financial support.** This research was supported by the Swedish Nuclear Fuel and Waste Management
442 Company.

443 Review statement.

444 **References**

445 Alexanderson, H., Hättstrand, M., Lindqvist, M. A., Sigfusdottir, T.: MIS 3 age of the Veiki moraine in
446 N Sweden - Dating the landform record of an intermediate-sized ice sheet in Scandinavia, Arctic,
447 Antarctic, and Alpine Research, 54, 239-261, 2022.

448 Balco, G., Stone, J. O., Lifton, N. A., Dunai, T. J.: A complete and easily accessible means of calculating
449 surface exposure ages or erosion rates from ^{10}Be and ^{26}Al measurements, Quaternary
450 Geochronology, 3, 174–195, 2008.

451 Berglund, M.: The Holocene shore displacement of Gästrikland, eastern Sweden: a contribution to
452 the knowledge of Scandinavian glacio-isostatic uplift, Journal of Quaternary Science, 20, 519–531,
453 2005.

454 Bergström, E.: Late Holocene distribution of lake sediment and peat in NE Uppland, Sweden, SKB R-
455 01-12, Svensk Kärnbränslehantering AB, 2001.

456 Bierman, P. R., Rood, D. H., Shakun, J. D., Portenga, E. W., Corbett, L. B.: Directly dating postglacial
457 Greenlandic land-surface emergence at high resolution using *in situ* ^{10}Be , Quaternary Research, 90,
458 110-126, 2018.

459 Blake, Jr., W.: Holocene emergence along the Ellesmere Island coast of northernmost Baffin Bay,
460 Norsk Geologisk Tidsskrift, 73, 147–160, 1993.

461 Borchers, B., Marrero, S., Balco, G., Caffee, M., Goehring, B., Lifton, N., Nishiizumi, K., Phillips, F.,
462 Schaefer, J., Stone, J.: Geological calibration of spallation production rates in the CRONUS Earth
463 project, Quaternary Geochronology, 31, 188–198, 2016.

464 Bradwell, T., Fabel, D., Clark, C. D., Chiverrell, R. C., Small, D., Smedley, R. K., Saher, M. H., Moreton,
465 S. G., Dove, D., Callard, S. L., Duller, G. A. T., Medialdea, A., Bateman, M. D., Burke, M. J., McDonald,
466 N., Gilgannon, S., Morgan, S., Roberts, D. H., Ó Cofaigh, C.: Pattern, style and timing of British-Irish Ice
467 Sheet advance and retreat over the last 45 000 years: evidence from NW Scotland and the adjacent
468 continental shelf, Journal of Quaternary Science, 36, 871–933, 2021.

469 Briner, J. P., Gosse, J. C., Bierman, P. R.: Applications of cosmogenic nuclides to Laurentide Ice Sheet
470 history and dynamics, Geological Society of America, Special Paper, 415, 29-41, 2006.

471

472 Briner, J. P., Lifton, N. A., Miller, G. H., Refsnider, K., Anderson, R. K., Finkel, R.: Using *in situ*
473 cosmogenic ^{10}Be , ^{14}C , and ^{26}Al to decipher the history of polythermal ice sheets, Quaternary
474 Geochronology, 19, 4–13, 2014.



- 475 Brunberg, L.: Clay-varve Chronology and Deglaciation during the Younger Dryas and Preboreal in the
476 Easternmost Part of the Middle Swedish Ice Marginal Zone, Department of Quaternary Research,
477 Quaternaria A2, Stockholm University, Stockholm, 1-94, 1995.
- 478 Dalton, A.S., Dulfer, H.E., Margold, M., Heyman, J., Clague, J.J., Froese, D.G., Gauthier, M.S., Hughes,
479 A.L.C., Jennings, C.E., Norris, S.L., Stoker, B.J.: Deglaciation of the north American ice sheet complex
480 in calendar years based on a comprehensive database of chronological data: NADI-1, Quaternary
481 Science Reviews, 321, 108345, 2023.
- 482 Dalton, A. S., Margold, M., Stokes, C. R., Tarasov, L., Dyke, A. S., Adams, R. S., Allard, S., Arends, H. E.,
483 Atkinson, N., Attig, J. W., Barnett, P. J., Barnett, R. L., Batterson, M., Bernatchez, P., Borns Jr., H. W.,
484 Breckenridge, A., Briner, J. P., Brouard, E., Campbell, J. E., Carlson, A. E., Clague, J. J., Curry, B. B.,
485 Daigneault, R. A., Dubé-Loubert, H., Easterbrook, D. J., Franzi, D. A., Friedrich, H. G., Funder, S.,
486 Gauthier, M. S., Gowan, A. S., Harris, K. L., Hétu, B., Hooyer, T. S., Jennings, C. E., Johnson, M. D.,
487 Kehew, A. E., Kelley, S. E., Kerr, D., King, E. L., Kjeldsen, K. K., Knaeble, A. R., Lajeunesse, P., Lakeman,
488 T. R., Lamothe, M., Larson, P., Lavoie, M., Loope, H. M., Lowell, T. V., Lusardi, B. A., Manz, L.,
489 McMartin, I., Nixon, F. C., Occhietti, S., Parkhill, M. A., Piper, D. J. W., Pronk, A. G., Richard, P. J. H.,
490 Ridge, J. C., Ross, M., Roy, M., Seaman, A., Shaw, J., Stea, R. R., Teller, J. T., Thompson, W. B.,
491 Thorleifson, L. H., Utting, D. J., Veillette, J. J., Ward, B. C., Weddle, T. K., Wright, H. E.: An updated
492 radiocarbon-based ice margin chronology for the last deglaciation of the North American Ice Sheet
493 Complex, Quaternary Science Reviews, 234, 106223, 2020.
- 494 De Geer, G.: The transbaltic extension of the Swedish Time Scale, Geografiska Annaler, 17, 533-549,
495 1935.
- 496 De Geer, G.: Geochronologia Suecica principles, Kungliga svenska vetenskapsakademien Handlingar,
497 III, Bd 18, 6, 1–367, 1940.
- 498 Dyke, A. S., Morris, T. F., Green, D. E. C., England, J.: Quaternary geology of Prince of Wales Island,
499 Arctic Canada, Geological Survey of Canada, Memoir, 433, 1–142, 1992.
- 500 Dyke, A. S., Andrews, J. T., Clark, P. U., England, J. H., Miller, G. H., Shaw, J., Veillette, J. J.: The
501 Laurentide and Innuitian ice sheets during the Last Glacial Maximum, Quaternary Science Reviews,
502 21, 9–31, 2002.
- 503 Fogwill, C., Turney, C., Golledge, N., Rood, D., Hippe, K., Wacker, L., Jones, R.: Drivers of abrupt
504 Holocene shifts in West Antarctic ice stream direction determined from combined ice sheet
505 modelling and geologic signatures. Antarctic Science, 26, 674–686, 2014.
- 506 Goehring, B. M., Schaefer, J. M., Schluechter, C., Lifton, N. A., Finkel, R. C., Jull, A. J. T., Akçar, N.,
507 Alley, R. B.: The Rhone Glacier was smaller than today for most of the Holocene, Geology, 39, 679–
508 682, 2011.
- 509 Gosse, J. C., Phillips, F. M.: Terrestrial *in situ* cosmogenic nuclides: theory and application, Quaternary
510 Science Reviews, 20, 1475–1560, 2001.
- 511 Greenwood, S. L., Simkins, L. M., Winsborrow, M. C. M., Bjarnadottir, L. R.: Exceptions to bed-
512 controlled ice sheet flow and retreat from glaciated continental margins worldwide, Science
513 Advances, 7, eabb6291, 2021.
- 514 Greenwood, S. L., Clason, C. C., Nyberg, J., Jakobsson, M., Holmlund, P.: The Bothnian Sea ice stream:
515 early Holocene retreat dynamics of the south-central Fennoscandian Ice Sheet, Boreas, 46, 346-362,
516 2017.



- 517 Hall A. M., Ebert K., Goodfellow B. W., Hättestrand C., Heyman J., Krabbendam M., Moon S., Stroeven
518 A. P.: Past and future impact of glacial erosion in Forsmark and Uppland. TR-19-07 Svensk
519 Kärnbränslehantering AB, 2019.
- 520 Hall, A. M., Krabbendam, M., van Boeckel, M., Goodfellow, B. W., Hättestrand, C., Heyman, J.,
521 Palamakumbura, R. N., Stroeven A. P., Näslund, J.-O.: Glacial ripping: geomorphological evidence
522 from Sweden for a new process of glacial erosion, *Geografiska Annaler*, 102, 333-353, 2020.
- 523 Hedenström, A., Risberg, J.: Shore displacement in northern Uppland during the last 6500 calendar
524 years, TR-03-17 Svensk Kärnbränslehantering AB, 2003.
- 525 Heyman, J., Stroeven, A. P., Harbor, J. M., Caffee, M. W.: Too young or too old: Evaluating
526 cosmogenic exposure dating based on an analysis of compiled boulder exposure ages, *Earth and
527 Planetary Science Letters*, 302, 71–80, 2011.
- 528 Hippe, K., Lifton, N. A.: Calculating isotope ratios and nuclide concentrations for *in situ* cosmogenic
529 ^{14}C Analyses, *Radiocarbon*, 56, 1167–1174, 2014.
- 530 Hippe, K., Ivy-Ochs, S., Kober, F., Zasadni, J., Wieler, R., Wacker, L., Kubik, P.W., Schlüchter, C.:
531 Chronology of Lateglacial ice flow reorganization and deglaciation in the Gotthard Pass area, Central
532 Swiss Alps, based on cosmogenic ^{10}Be and *in situ* ^{14}C , *Quaternary Geochronology*, 19, 14–26, 2014.
- 533 Hughes, A. L. C., Gyllencreutz, R., Lohne, Ø. S., Mangerud, J., Svendsen, J. I.: The last Eurasian ice
534 sheets – a chronological database and time-slice reconstruction, *DATED-1, Boreas*, 45, 1–45, 2016.
- 535 Ivy-Ochs, S., Kober, F.: Surface exposure dating with cosmogenic nuclides, *Quaternary Science
536 Journal*, 57, 157–189, 2008.
- 537 Kleman, J., Hättestrand, M., Borgström, I., Preusser, F., Fabel, D.: The Idre marginal moraine—an
538 anchorpoint for Middle and Late Weichselian ice sheet chronology, *Quaternary Science Advances*, 2,
539 100010, 2020.
- 540 Kleman, J., Stroeven, A. P., Lundqvist, J.: Patterns of Quaternary ice sheet erosion and deposition in
541 Fennoscandia and a theoretical framework for explanation, *Geomorphology*, 97, 73–90, 2008.
- 542 Koester, A., Lifton, N. A.: Technical note: A software framework for calculating compositionally
543 dependent *in situ* ^{14}C production rates, *Geochronology*, 5, 21–33, 2023.
- 544 Lal, D.: Cosmic ray labeling of erosion surfaces: *in situ* nuclide production rates and erosion rates,
545 *Earth and Planetary Science Letters*, 104, 424–439, 1991.
- 546 Lambeck, K., Purcell, A., Zhao, J., Svensson, N.-O.: The Scandinavian Ice Sheet: from MIS 4 to the end
547 of the Last Glacial Maximum, *Boreas*, 39, 410-435, 2010.
- 548 Lambeck, K., Smither, C., Johnston, P.: Sea-level change, glacial rebound and mantle viscosity for
549 northern Europe, *Geophysical Journal International*, 134, 102-134, 1998.
- 550 Lidberg, M., Johansson, J. M., Scherneck, H.-G., Milne, G. A.: Recent results based on continuous GPS
551 observations of the GIA process in Fennoscandia from BIFROST, *Journal of Geodynamics*, 50, 8–18,
552 2010.
- 553 Lifton, N.: Implications of two Holocene time-dependent geomagnetic models for cosmogenic nuclide
554 production rate scaling, *Earth and Planetary Science Letters*, 433, 257–268, 2016.



- 555 Lifton, N., Caffee, M., Finkel, R., Marrero, S., Nishiizumi, K., Phillips, F. M., Goehring, B., Gosse, J.,
556 Stone, J., Schaefer, J., Theriault, B.: *In situ* cosmogenic nuclide production rate calibration for the
557 CRONUS-Earth project from Lake Bonneville, Utah, shoreline features, *Quaternary Geochronology*,
558 26, 56–69, 2015.
- 559 Lifton, N., Sato, T., and Dunai, T. J.: Scaling *in situ* cosmogenic nuclide production rates using
560 analytical approximations to atmospheric cosmic-ray fluxes, *Earth and Planetary Science Letters*, 386,
561 149–160, 2014.
- 562 Lifton, N., Wilson, J., Koester, A.: Technical note: Studying Li-metaborate fluxes and extraction
563 protocols with a new, fully automated *in situ* cosmogenic ^{14}C processing system at PRIME Lab,
564 *Geochronology*, 5, 361–375, 2023.
- 565 Long, A. J., Woodroffe, S. A., Roberts, D. H., Dawson, S.: Isolation basins, sea-level changes and the
566 Holocene history of the Greenland Ice Sheet, *Quaternary Science Reviews*, 30, 3748–3768, 2011.
- 567 Lönnqvist, M., Hökmark, H.: Approach to estimating the maximum depth for glacially induced
568 hydraulic jacking in fractured crystalline rock at Forsmark, Sweden, *Journal of Geophysical Research:*
569 *Earth Surface*, 118, 1777–1791, 2013.
- 570 Lupker, M., Hippe, K., Wacker, L., Kober, F., Maden, C., Braucher, R., Bourlès, D., Romani, J. R. V.,
571 Wieler, R.: Depth-dependence of the production rate of *in situ* ^{14}C in quartz from the Leymon High
572 core, Spain, *Quaternary Geochronology*, 28, 80–87, 2015.
- 573 Margold, M., Gosse, J. C., Hidy, A. J., Woywitka, R. J., Young, J. M., Froese, D.: Beryllium-10 dating of
574 the Foothills Erratics Train in Alberta, Canada, indicates detachment of the Laurentide Ice Sheet from
575 the Rocky Mountains at ~ 15 ka, *Quaternary Research*, 92, 469–482, 2019.
- 576 Marrero, S. M., Phillips, F. M., Caffee, M. W., Gosse, J. C.: CRONUS-Earth cosmogenic ^{36}Cl calibration,
577 *Quaternary Geochronology*, 31, 199–219, 2016.
- 578 Matmon, A., Crouvi, O., Enzel, Y., Bierman, P., Larsen, J., Porat, N., Amit, R., Caffee, M.: Complex
579 exposure histories of chert clasts in the late Pleistocene shorelines of Lake Lisan, southern Israel.
580 *Earth Surface Processes and Landforms* 28, 493–506, 2003.
- 581 Miller, G. H., Briner, J. P., Lifton, N. A., Finkel, R. C.: Limited ice-sheet erosion and complex exposure
582 histories derived from *in situ* cosmogenic ^{10}Be , ^{26}Al , ^{14}C on Baffin Island, Arctic Canada, *Quaternary*
583 *Geochronology*, 1, 74–85, 2006.
- 584 Moon, S., Perron, J. T., Martel, S.J., Goodfellow, B.W., Mas Ivars, D., Hall, A., Heyman, J., Munier, R.,
585 Näslund, J.-O., Simeonov, A., Stroeven, A.P.: Present-day stress field influences bedrock fracture
586 openness deep into the subsurface. *Geophysical Research Letters* 47, e2020GL090581, 2020.
- 587 Norris, S. L., Tarasov, L., Monteath, A. J., Gosse, J. C., Hidy, A. J., Margold, M., Froese, D. G.: Rapid
588 retreat of the southwestern Laurentide Ice Sheet during the Bølling-Allerød interval, *Geology*, 50,
589 417–421, 2022.
- 590 Påsse, T., Andersson, L.: Shore-level displacement in Fennoscandia calculated from empirical data,
591 *GFF*, 127, 253–268, 2005.
- 592 Patton, H., Hubbard, A., Andreassen, K., Auriac, A., Whitehouse, P. L., Stroeven, A. P., Shackleton, C.,
593 Winsborrow, M., Heyman, J., Hall, A. M.: Deglaciation of the Eurasian ice sheet complex, *Quaternary*
594 *Science Reviews*, 169, 148–172, 2017.



- 595 Patton, H., Hubbard, A., Andreassen, K., Winsborrow, M., Stroeven, A.P.: The build-up, configuration,
596 and dynamical sensitivity of the Eurasian ice-sheet complex to Late Weichselian climatic and oceanic
597 forcing, *Quaternary Science Reviews*, 153, 97–121, 2016.
- 598 Patton, H., Hubbard, A., Heyman, J., Alexandropoulou, N., Lasabuda, A. P. E., Stroeven, A.P., Hall,
599 A.M., Winsborrow, M., Sugden, D.E., Kleman, J., Andreassen, K.: The extreme yet transient nature of
600 glacial erosion, *Nature Communications* 13, 7377, 2022.
- 601 Pendleton, S., Miller, G., Lifton, N., Young, N.: Cryosphere response resolves conflicting evidence for
602 the timing of peak Holocene warmth on Baffin Island, Arctic Canada, *Quaternary Science*
603 *Reviews*, 216, 107–115, 2019.
- 604 Phillips, F. M., Argento, D. C., Balco, G., Caffee, M. W., Clem, J., Dunai, T. J., Finkel, R., Goehring, B.,
605 Gosse, J. C., Hudson, A. M., Jull, A. J. T., Kelly, M. A., Kurz, M., Lal, D., Lifton, N., Marrero, S. M.,
606 Nishiizumi, K., Reedy, R. C., Schaefer, J., Stone, J. O. H., Swanson, T., Zreda, M. G.: The CRONUS-Earth
607 Project: A synthesis, *Quaternary Geochronology*, 31, 119–154, 2016.
- 608 Rainio, H., Kejonen, A., Kielosto, S., Lahermo, P.: Avancerade inlandsisen på nytt också till
609 Mellanfinska randformationen? *Geologi*, 38, 95–109, 1986.
- 610 Regnéll, C., Becher, G. P., Öhrling, C., Greenwood, S. L., Gyllencreutz, R., Blomdin, R., Brendryen, J.,
611 Goodfellow, B. W., Mikko, H., Ransed, G., Smith, C.: Ice-dammed lakes and deglaciation history of the
612 Scandinavian Ice Sheet in central Jämtland, Sweden, *Quaternary Science Reviews*, 314, 108219, 2023.
- 613 Risberg, J.: Strandförskjutningen i nordvästra Uppland under subboreal tid. In Segerberg, A. Bälunge
614 mossar: kustbor i Uppland under yngre stenålder, PhD Thesis. Uppsala University, Appendix 4. (in
615 Swedish), 1999.
- 616 Robertsson, A.-M., Persson, C.: Biostratigraphical studies of three mires in northern Uppland,
617 Sweden, *Sveriges geologiska undersökning*, (Serie C 821.), 1989.
- 618 Romundset, A., Bondevik, S., Bennike, O.: Postglacial uplift and relative sea level changes in
619 Finnmark, northern Norway, *Quaternary Science Reviews*, 30, 2398–2421, 2011.
- 620 Schildgen, T. F., Phillips, W. M., Purves, R. S.: Simulation of snow shielding corrections for cosmogenic
621 nuclide surface exposure studies, *Geomorphology*, 64, 67–85, 2005.
- 622 Schimmelpfennig, I., Schaefer, J. M., Goehring, B. M., Lifton, N., Putnam, A. E., Barrell, D. J.:
623 Calibration of the *in situ* cosmogenic ^{14}C production rate in New Zealand's Southern Alps, *Journal of*
624 *Quaternary Science*, 27, 671–674, 2012.
- 625 Schimmelpfennig, I., Schaefer, J. M., Lamp, J., Godard, V., Schwartz, R., Bard, E., Tuna, T., Akçar, N.,
626 Schlüchter, C., Zimmerman, S., and ASTER Team: Glacier response to Holocene warmth inferred from
627 *in situ* ^{10}Be and ^{14}C bedrock analyses in Steingletscher's forefield (central Swiss Alps), *Climate of the*
628 *Past*, 18, 23–44, 2022.
- 629 Schweinsberg, A. D., Briner, J. P., Miller, G. H., Lifton, N. A., Bennike, O., & Graham, B. L.: Holocene
630 mountain glacier history in the Sukkertoppen Iskappe area, southwest Greenland, *Quaternary*
631 *Science Reviews*, 197, 142–161, 2018.
- 632 SGU: Högsta Kustlinjen (in Swedish) [https://resource.sgu.se/dokument/produkter/hogsta-kustlinjen-](https://resource.sgu.se/dokument/produkter/hogsta-kustlinjen-beskrivning)
633 [beskrivning](https://resource.sgu.se/dokument/produkter/hogsta-kustlinjen-beskrivning) (Geological Survey of Sweden), 2015.



- 634 Simkins, L. M., Simms, A. R., DeWitt, R.: Relative sea-level history of Marguerite Bay, Antarctic
635 Peninsula derived from optically stimulated luminescence-dated beach cobbles, *Quaternary Science*
636 *Reviews*, 77, 141–155, 2013.
- 637 SKB: Post-closure safety for the final repository for spent nuclear fuel at Forsmark – Climate and
638 climate-related issues, PSAR version, TR-20-12, Svensk Kärnbränslehantering AB, 2020.
- 639 SKB: Post-closure safety for the final repository for spent nuclear fuel at Forsmark – Main report,
640 PSAR version. SKB TR-21-01, Svensk Kärnbränslehantering AB, 2022.
- 641 Steffen, H., Wu, P.: Glacial isostatic adjustment in Fennoscandia - A review of data and modeling,
642 *Journal of Geodynamics*, 52, 169–204, 2011.
- 643 Steinemann, O., Ivy-Ochs, S., Hippe, K., Christl, M., Haghpor, N., and Synal, H. A.: Glacial erosion by
644 the Trift glacier (Switzerland): Deciphering the development of riegels, rock basins and gorges,
645 *Geomorphology*, 375, 107533, 2021.
- 646 Stephens, M. B., Jansson, N. F.: Chapter 6, Paleoproterozoic (1.9–1.8 Ga) syn-orogenic magmatism,
647 sedimentation and mineralization in the Bergslagen lithotectonic unit, Svecokarelian orogen. In M B
648 Stephens & J Bergman Weihed (eds.): Sweden: Lithotectonic Framework, Tectonic Evolution and
649 Mineral Resources, *Geological Society of London Memoirs*, 50, 105–206, 2020.
- 650 Stroeve, A. P., Hättstrand, C., Kleman, J., Heyman, J., Fabel, D., Fredin, O., Goodfellow, B. W.,
651 Harbor, J. M., Jansen, J. D., Olsen, L., Caffee, M. W., Fink, D., Lundqvist, J., Rosqvist, G. C., Strömberg,
652 B., Jansson, K. N.: Deglaciation of Fennoscandia, *Quaternary Science Reviews*, 147, 91–12, 2016.
- 653 Stroeve, A.P., Heyman, J., Fabel, D., Björck, S., Caffee, M.W., Fredin, O., Harbor, J.M.: A new
654 Scandinavian reference ^{10}Be production rate, *Quaternary Geochronology*, 29, 104–115, 2015.
- 655 Strömberg, B.: Late Weichselian deglaciation and clay varve chronology in east-central Sweden,
656 *Sveriges geologiska undersökning (Ser. Ca 73)*, 1989.
- 657 Strömberg, B.: Younger Dryas deglaciation at Mt. Billingen, and clay varve dating of the Younger
658 Dryas/Preboreal transition, *Boreas*, 23, 177–193, 1994.
- 659 Wohlfarth, B., Björck, S., Possnert, G.: The Swedish Time Scale: a potential calibration tool for the
660 radiocarbon time scale during the late Weichselian, *Radiocarbon*, 37, 347–359, 1995.
- 661 Young, N. E., Lesnek, A. J., Cuzzone, J. K., Briner, J. P., Badgley, J. A., Balter-Kennedy, A., Graham, B.
662 L., Cluett, A., Lamp, J. L., Schwartz, R., Tuna, T., Bard, E., Caffee, M. W., Zimmerman, S. R. H.,
663 Schaefer, J. M.: *In situ* cosmogenic ^{10}Be – ^{14}C – ^{26}Al measurements from recently deglaciated bedrock as
664 a new tool to decipher changes in Greenland Ice Sheet size, *Climate of the Past*, 17, 419–450, 2021.
- 665 Young, N. E., Schaefer, J. M., Goehring, B., Lifton, N., Schimmelpennig, I., Briner, J. P.: West
666 Greenland and global *in situ* ^{14}C production-rate calibrations, *Journal of Quaternary Science*, 29, 401–
667 406, 2014.